Society for
Mathematical
Biology

ORIGINAL ARTICLE

Effect of Human Mobility on the Spatial Spread of Airborne Diseases: An Epidemic Model with Indirect Transmission

Jummy F. David[1,3,4] · **Sarafa A. Iyaniwura**[2]

Abstract

We extended a class of coupled PDE–ODE models for studying the spatial spread of airborne diseases by incorporating human mobility. Human populations are modeled with patches, and a Lagrangian perspective is used to keep track of individuals' places of residence. The movement of pathogens in the air is modeled with linear diffusion and coupled to the SIR dynamics of each human population through an integral of the density of pathogens around the population patches. In the limit of fast diffusion pathogens, the method of matched asymptotic analysis is used to reduce the coupled PDE–ODE model to a nonlinear system of ODEs for the average density of pathogens in the air. The reduced system of ODEs is used to derive the basic reproduction number and the final size relation for the model. Numerical simulations of the full PDE–ODE model and the reduced system of ODEs are used to assess the impact of human mobility, together with the diffusion of pathogens on the dynamics of the disease. Results from the two models are consistent and show that human mobility significantly affects disease dynamics. In addition, we show that an increase in the diffusion rate of pathogen leads to a lower epidemic.

Keywords Human mobility · Heterogeneous mixing · Epidemics · Airborne disease · Indirect transmission · Asymptotic analysis · Green's function

✉ Jummy F. David
jummy30@yorku.ca

✉ Sarafa A. Iyaniwura
iyaniwura@math.ubc.ca

1   Department of Mathematics and Statistics, York University, Toronto, ON, Canada

2   Department of Mathematics and Institute of Applied Mathematics, University of British Columbia, Vancouver, BC, Canada

3   Laboratory for Industrial and Applied Mathematics, York University, Toronto, ON, Canada

4   Fields-CQAM Laboratory of Mathematics for Public Health (MfPH), York University, Toronto, ON, Canada

⌂ Springer

1 Introduction

Airborne transmission of infectious diseases has been a subject of increasing interest in recent times. Analyzing the potential risk of airborne transmission by incorporating human mobility into studies can provide important information for designing safe environments with appropriate level of controls for mitigating risks. Many airborne and waterborne diseases are transmitted directly via host–host and/or indirectly through the host–source–host route (Boone and Gerba 2007; Trisha et al. 2021). Airborne diseases such as measles, influenza, and tuberculosis are primarily transmitted from human–environment–human (indirect transmission pathway) and can as well be transmitted from human–human (direct transmission pathway) (Hartley et al. 2006; Nelson et al. 2009; Noakes and Sleigh 2009). The emergence of severe acute respiratory syndrome (SARS) in 2002–2003 caused a public health concern (Steven et al. 2003)with a highly infectious coronavirus causing the SARS disease (Lipsitch et al. 2003) known to primarily spread through localized contact with contaminated droplets. In addition, retrospective studies including but not limited to Li et al. (2005) suggested that airborne dispersal may play an important role in the transmission of the disease with evidence showing that uninfected individuals were infected without enough close contact with an infectious individual (Scales Damon et al. 2003).

In the context of models for infectious diseases transmission, the Lagrangian approach offers a theoretical framework that explicitly tracks the heterogeneity of host population and mobility (Fred et al. 2019). Despite the complexity of explicitly considering the mixing patterns and connections that exist between local communities and different regions, the Lagrangian method used for residence time has shown its ability to analytically explain the failure of feasible mobility restriction measures and their impact on disease transmission (Brauer 2012; Fred et al. 2019). Several mathematical models that studied heterogeneity and different mobility scenarios have been explored within the heterogeneous mixing framework (Brauer 2008b, 2012; Fred et al. 2019). However, none of these studies considered epidemic models with diffusion of pathogens and/or indirect transmission route using our approach of a coupled PDE–ODE model.

In fact, many authors including but not limited to the authors in David et al. (2020), Noakes and Sleigh (2009), Wang and Wang (2021), Yamazaki et al. (2021) and Zhang et al. (2016) extensively studied and analyzed the transmission of airborne and waterborne diseases using different modeling approaches. For example, (Noakes and Sleigh 2009) used a stochastic version of the Wells–Riley's model coupled with a simple zonal ventilation model that allowed for the effects of small populations applicable in healthcare settings. They demonstrated the role of airflow and population size on the risk of infection and the importance of stochastic effects, especially in small populations, was emphasized. Their approach enabled an understanding of the possible spatial transmission of infection that allowed design and operational control strategies to be explored without explicitly modeling the role of diffusion. Wang and Wang (2021) developed a multipatch cholera epidemic model to assess disease dynamics in a periodic environment. They illustrated the impact of asymptomatic infections and population dispersal on the spread of cholera. Although useful results were obtained, their modeling framework did not show the effect of diffusion and human mobil-

ity on the transmission of the disease. Similarly, (Yamazaki et al. 2021) proposed a new reaction–convection–diffusion model to study the impact of cholera transmission among humans using a second-order differential operator. This model differs from the current study in structure and dynamics in that a second-order differential operator was used without addressing the potential effect of the movement of humans between patches. Furthermore, (Zhang et al. 2016) formulated a reaction–diffusion waterborne pathogen model to investigate the influence of diffusion, spatial heterogeneity, and multiple transmission pathways on the spread of waterborne disease. While the work done in Zhang et al. (2016) considered the influence of dispersal using a different model, the spatiotemporal spread of the disease with the impact of human mobility was not taken into consideration. In addition, the work of David et al. (2020) which is a prequel to the current study used a novel PDE–ODE model to study the spatial spread of airborne diseases between homogeneous populations. The current work extends the work done in David et al. (2020) by explicitly modeling the role of human mobility.

In light of the aforementioned studies, we thought it could be possible to consider a more realistic but simpler scenario (in the case of superspreaders) rather than the detailed network or PDE models. To model the effect of human mobility with heterogeneous mixing, one may assume that the population is divided into subgroups with different activity levels. To the best of our knowledge, no previous studies and articles considered our modeling approach of using a coupled PDE–ODE system in assessing the role of human mobility and heterogeneous mixing on the transmission of airborne diseases. This work aims to indirectly overcome the complications faced by using a PDE model. We base our analytical results on the reproduction number and the epidemic final size relation in a heterogeneous mixing environment. Our results are computed using a nonlinear system of ODEs derived from the coupled PDE–ODE using strong localized perturbation theory in the limit of fast diffusing pathogens. We use the Lagrangian method to track an individual's place of residence at all time following the approach in Bichara et al. (2015), Brauer (2008b), Fred et al. (2019), Carlos et al. (2016), Espinoza et al. (2016) and Funke (2018). This allows us to theoretically and numerically evaluate how human movement between patches (regions) affect the spread of diseases. Our extended model which includes human mobility and a diffusion term may be an alternative way to study the spread of airborne diseases in an heterogeneous mixing environment.

The rest of the paper is structured as follows. In Sect. 2, we extend the coupled PDE–ODE model developed in David et al. (2020) by incorporating human mobility using the Lagrangian method. We non-dimensionalize the extended model in Sect. 2.1 and use matched asymptotic expansions method to reduce the dimensionless coupled model to a nonlinear system of ODEs in the limit of fast diffusing pathogens. In Sects. 3.1 and 3.2, for a scenario with two populations, the reduced ODE model is used to compute the basic reproduction number and final size relation of the epidemic, respectively. The coupled PDE–ODE model together with the reduced system of ODEs is used to numerically study the effect of different human mobility patterns on the disease dynamics for a two-patch scenario. A brief discussion of results and possible future directions concludes the paper in Sect. 4.

2 Mathematical Model

Here, we represent human populations with localized patches that have partially trans-
mitting boundaries through which pathogens are shed into the atmosphere by infected
individuals. These pathogens diffuse and decay at a constant rate in the air. A sus-
ceptible individual becomes infected by coming in contact with pathogens (*indirect
transmission pathway*). We assume that the spread of infection in each population
patch depends on the density of pathogens around the patch, and did not explicitly
model pathogens within the patches. Similarly, we model human movement between
patches using a Lagrangian method. Let $\Omega \subset \mathbb{R}^2$ be our 2-D bounded domain of
interest containing m population patches represented, by Ω_j for $j = 1, \dots, m$, which
are separated by an $O(1)$ distance. In the region between the patches $\Omega \setminus \cup_{j=1}^m \Omega_j$
(bulk region), the density of pathogens $\mathcal{P}(\boldsymbol{X}, T)$ satisfies

$$\frac{\partial \mathcal{P}}{\partial T} = D_B \,\Delta \mathcal{P} - \delta \mathcal{P}, \quad T > 0, \quad \boldsymbol{X} \in \Omega \setminus \cup_{j=1}^m \Omega_j; \tag{1a}$$

$$\partial_{n_{\boldsymbol{X}}} \mathcal{P} = 0, \quad \boldsymbol{X} \in \partial\Omega; \qquad D_B \,\partial_{n_{\boldsymbol{X}_j}} \mathcal{P} = -r_j \,\mathcal{I}_j, \quad \boldsymbol{X} \in \partial\Omega_j, \qquad j = 1, \dots, m, \tag{1b}$$

where $D_B > 0$ and $\delta > 0$, respectively, represent the dimensional diffusion coefficient
and decay rate of pathogens in the bulk region, $r_j > 0$ is the dimensional shedding
rate of pathogen by an infected individual in the jth patch, and $\partial_{n_{\boldsymbol{X}}}$ is the outer normal
derivative on the boundary of the patches pointing into the bulk region.

First, we assume that the population of the entire system is constant throughout the
epidemic period, that is, $N = \sum_{j=1}^m N_j$. Here, γ_{ji} denote the fraction of residents of
patch j that are in patch i, where $\sum_{i=1}^m \gamma_{ji} = 1$ for $j = 1, \dots, m$. The parameters
μ_j and α_j are the dimensional transmission and recovery rates, respectively, for indi-
viduals in the jth patch, and p_c is a typical value for the density of pathogens. The
dynamics of the diffusing pathogens in the bulk region is coupled to the population
dynamics of the jth patch as follows

$$\frac{dS_j}{dT} = -\sum_{i=1}^m \mu_i \,S_j \,\gamma_{ji} \int_{\partial\Omega_i} (\mathcal{P}/p_c) \,dS_{\boldsymbol{X}i}; \tag{1c}$$

$$\frac{d\mathcal{I}_j}{dT} = \sum_{i=1}^m \mu_i \,S_j \,\gamma_{ji} \int_{\partial\Omega_i} (\mathcal{P}/p_c) \,dS_{\boldsymbol{X}i} - \alpha_j \mathcal{I}_j; \tag{1d}$$

$$\frac{d\mathcal{R}_j}{dT} = \alpha_j \mathcal{I}_j, \qquad j = 1, \dots, m, \tag{1e}$$

where S_j, $\mathcal{I}_j$, and $\mathcal{R}_j$ are the susceptible, infected, and recovered/removed population
in the jth patch, respectively, with the total population at time T written as $\mathcal{N}_j(T) = S_j(T) + \mathcal{I}_j(T) + \mathcal{R}_j(T)$.

The integrals in (1c) and (1d) are over the boundary of the jth patch and are used
to account for the total density of pathogens around the patch. These terms show that
the spread of infection within a patch depends on the density of pathogens around

the patch. It is important to emphasize that our model does not explicitly account for pathogens within the patches. The Robin boundary condition $D_B \, \partial_{n_X} \mathcal{P} = -r_j \, \mathcal{I}_j$ on the boundary of the jth patch accounts for the amount of pathogens shed into the atmosphere by infected individuals in the patch. This condition shows that the amount of pathogens shed into the atmosphere from the jth patch depends on the population of infected individuals in the patch.

2.1 Non-dimensionalization of the Coupled PDE–ODE Model

Next, we non-dimensionalize the coupled PDE–ODE model (1). The dimensions of the variables and parameters of the model are defined as follows:

$$
[\mathcal{P}] = \frac{\text{pathogens}}{(\text{length})^2}, \qquad [D_B] = \frac{(\text{length})^2}{\text{time}}, \quad [p_c] = \text{pathogens}, \quad [T] = \text{time},
$$

$$
[\boldsymbol{X}] = \text{length}, \quad [\mu_j] = \frac{\text{length}}{\text{time}}, \quad [\mathcal{N}_j] = [\mathcal{S}_j] = [\mathcal{I}_j] = [\mathcal{R}_j] = \text{individuals},
$$

$$
[r_j] = \frac{\text{pathogens}}{\text{individual} \ \times \ \text{time} \times \text{length}}, \quad [\delta] = [\alpha_j] = \frac{1}{\text{time}}, \quad i, j = 1, \ldots, m.
$$
(2)

where $[z]$ represents the dimension of z. We assume that the population patches are circular with common radius ρ, which is small compared to the length-scale L of the domain Ω, and introduce a small scaling parameter $\varepsilon = \rho/L \ll 1$. The dimensionless variables are defined as follows

$$
P = \frac{L^2}{p_c}\mathcal{P}, \quad S_j = \frac{\mathcal{S}_j}{\mathcal{N}_j}, \quad I_j = \frac{\mathcal{I}_j}{\mathcal{N}_j}, \quad R_j = \frac{\mathcal{R}_j}{\mathcal{N}_j}, \quad \boldsymbol{x} = \frac{\boldsymbol{X}}{L}, \quad t = \delta \, T. \tag{3}
$$

so that S_j, I_j, and R_j are the proportion of susceptible, infected, and recovered/removed individuals in the jth patch, respectively, and $P \equiv P(\boldsymbol{x}, t)$ is the dimensionless density of pathogens in the bulk region. Upon substituting (3) into (1), we derive that $P(\boldsymbol{x}, t)$ satisfies

$$
\frac{\partial P}{\partial t} = D \, \Delta \, P - P, \quad t > 0, \quad \boldsymbol{x} \in \Omega \setminus \cup_{j=1}^{m} \Omega_{\varepsilon j}; \tag{4a}
$$

$$
\partial_{n_{\boldsymbol{x}}} P = 0, \quad \boldsymbol{x} \in \partial\Omega; \qquad D \, \partial_{n_{\boldsymbol{x}}} P = -r_j \left(\frac{\mathcal{N}_j L}{\delta \, p_c} \right) I_j, \quad \boldsymbol{x} \in \partial\Omega_{\varepsilon j}, \quad j = 1, \ldots, m,
$$
(4b)

where $D \equiv D_B/(\delta \, L^2)$ is the effective diffusion rate of pathogens in the bulk region. From the ODE system ((1c)–(1e)), we derive the dimensionless system of ODEs for the population dynamics of the jth patch as

$$\frac{dS_j}{dt} = -\sum_{i=1}^{m} \left(\frac{\mu_i}{\delta L}\right) S_j \gamma_{ji} \int_{\partial \Omega_{\varepsilon i}} P \, ds_{\boldsymbol{x}} \, ;$$

$$\frac{dI_j}{dt} = \sum_{i=1}^{m} \left(\frac{\mu_i}{\delta L}\right) S_j \gamma_{ji} \int_{\partial \Omega_{\varepsilon i}} P \, ds_{\boldsymbol{x}} - \phi_j I_j \, ; \tag{5}$$

$$\frac{dR_j}{dt} = \phi_j I_j, \quad j = 1, \ldots, m,$$

where $\phi_j = \alpha_j/\delta$ is the dimensionless recovery rate and $\Omega_{\varepsilon j} = \{\boldsymbol{x} : |\boldsymbol{x}_j - \boldsymbol{x}| < \varepsilon\}$ represents the jth patch of radius $\varepsilon \ll 1$ with center at $\boldsymbol{x}_j$. Note that we have used the scaling $dS_{\boldsymbol{X}} = L \, ds_{\boldsymbol{x}}$ in the integrals on the boundary of the patches. We set

$$\frac{\beta_j}{2\pi\varepsilon} = \frac{\mu_j}{\delta L} \quad \text{and} \quad \frac{\sigma_j}{2\pi\varepsilon} = r_j \frac{N_j L}{\delta \, p_c}, \tag{6}$$

where β_j and σ_j are $O(1)$. We have assumed that $(\mu_j/\delta L)$ and $r_j (N_j L/\delta \, p_c)$ are $O(1/\varepsilon)$ in order to effectively capture the density of pathogens shed into the bulk region by infected individuals in each patch, since the patches are relatively small compared to the length-scale of the domain. This re-scaling enables us to write the dimensionless transmission and shedding rates, β_j and σ_j, respectively, as functions of the circumference of the jth patch. Upon substituting (6) into (4) and (5), we obtain that the dimensionless density of the pathogens $P(\boldsymbol{x}, t)$ satisfies

$$\frac{\partial P}{\partial t} = D \, \Delta \, P - P, \quad t > 0, \quad \boldsymbol{x} \in \Omega \setminus \cup_{j=1}^{m} \Omega_{\varepsilon j}; \tag{7a}$$

$$\partial_{n_{\boldsymbol{x}}} P = 0, \quad \boldsymbol{x} \in \partial\Omega; \quad 2\pi\varepsilon D \, \partial_{n_{\boldsymbol{x}}} P = -\sigma_j I_j, \quad \boldsymbol{x} \in \partial\Omega_{\varepsilon j}, \quad j = 1, \ldots, m, \tag{7b}$$

which is coupled to the dimensionless SIR dynamics of the jth patch as follows

$$\frac{dS_j}{dt} = -\frac{1}{2\pi\varepsilon} \sum_{i=1}^{m} \beta_i S_j \gamma_{ji} \int_{\partial\Omega_{\varepsilon j}} P \, ds_{\boldsymbol{x}};$$

$$\frac{dI_j}{dt} = \frac{1}{2\pi\varepsilon} \sum_{i=1}^{m} \beta_i S_j \gamma_{ji} \int_{\partial\Omega_{\varepsilon j}} P \, ds_{\boldsymbol{x}} - \phi_j I_j; \tag{7c}$$

$$\frac{dR_j}{dt} = \phi_j I_j, \quad j = 1, \ldots, m,$$

where

$$\beta_j = \frac{2\pi\varepsilon}{\delta L} \mu_j, \quad \sigma_j = \frac{2\pi\varepsilon}{\delta \, p_c} r_j N_j L \quad \text{and} \quad \phi_j = \frac{\alpha_j}{\delta}. \tag{8}$$

are the dimensionless transmission, shedding, and recovery rates for the jth patch, respectively. Table 1 shows all parameters and their respective descriptions.

Next, we study the dimensionless coupled model (7) in the limit of fast diffusing pathogens, where $D = O(\nu^{-1}) \gg 1$, with $\nu = -1/\log_e(\varepsilon)$ and $\varepsilon \ll 1$, using the method of matched asymptotic expansions. We define

$$D = \frac{D_0}{\nu}, \quad \text{where} \quad D_0 = O(1) \quad \text{and} \quad \nu = -\frac{1}{\log_e(\varepsilon)} \ll 1. \tag{9}$$

Substituting $D = D_0/\nu$ into (7a) and (7b), we obtain

$$\frac{\partial P}{\partial t} = \frac{D_0}{\nu} \Delta P - P, \quad t > 0, \quad \boldsymbol{x} \in \Omega \setminus \cup_{j=1}^{m} \Omega_{\varepsilon j}; \tag{10a}$$

$$\partial_{n_{\boldsymbol{x}}} P = 0, \quad \boldsymbol{x} \in \partial\Omega; \quad 2\pi\varepsilon \frac{D_0}{\nu} \partial_{n_{\boldsymbol{x}}} P = -\sigma_j I_j, \quad \boldsymbol{x} \in \partial\Omega_{\varepsilon j}, \quad j = 1, \dots, m, \tag{10b}$$

Following the approach of David et al. (2020), we derive a two-term asymptotic expansion in terms of ν for the density of pathogens in the bulk region given by

$$P = P_0 + \frac{\nu}{D_0} \sum_{i=1}^{m} \sigma_i I_i \, G(\boldsymbol{x}; \boldsymbol{x}_i) + \dots, \tag{11}$$

where $P_0 \equiv P_0(t)$ is the average density of pathogens in the bulk region which satisfies

$$\frac{\mathrm{d}P_0}{\mathrm{d}t} = -P_0 + \frac{1}{|\Omega|} \sum_{j=1}^{m} \sigma_j I_j, \tag{12}$$

and $G(\boldsymbol{x}; \boldsymbol{x}_j)$ is the Neumann's Green function satisfying

$$\Delta G = \frac{1}{|\Omega|} - \delta(\boldsymbol{x} - \boldsymbol{x}_j), \quad \boldsymbol{x} \in \Omega; \quad \partial_n G = 0, \quad \boldsymbol{x} \in \partial\Omega; \tag{13a}$$

$$G(\boldsymbol{x}; \boldsymbol{x}_j) \sim -\frac{1}{2\pi} \log_e |\boldsymbol{x} - \boldsymbol{x}_j| + \mathfrak{R}_j, \quad \text{as} \quad \boldsymbol{x} \to \boldsymbol{x}_j, \quad \text{and} \quad \int_\Omega G \, \mathrm{d}\boldsymbol{x} = 0, \tag{13b}$$

with regular part $\mathfrak{R}_j \equiv \mathfrak{R}(\boldsymbol{x}_j)$. Similarly, near the jth population patch, we derive

$$Q_j = \left(P_0(t) + \frac{\sigma_j I_j}{2\pi D_0} \right) + \frac{\nu}{D_0} \left[-\left(\frac{\sigma_j I_j}{2\pi} \right) \log_e \left(\frac{|\boldsymbol{x} - \boldsymbol{x}_j|}{\varepsilon} \right) \right.$$

$$\left. + \sigma_j I_j \mathfrak{R}_j + \sum_{i \neq j}^{m} \sigma_i I_i \, G(\boldsymbol{x}_j; \boldsymbol{x}_i) \right] + \cdots, \quad j = 1, \dots, m, \tag{14}$$

On the boundary of the jth patch, where $|\boldsymbol{x} - \boldsymbol{x}_j| = \varepsilon$, (14) reduces to

$$Q_j = \left(P_0(t) + \frac{\sigma_j I_j}{2\pi D_0} \right)$$

$$+\frac{\nu}{D_0}\left(\sigma_j I_j \Re_j + \sum_{i \neq j}^{m} \sigma_i I_i \, G(\boldsymbol{x}_j; \boldsymbol{x}_i)\right) + \ldots, \qquad j = 1, \ldots, m, \quad (15)$$

To couple the dynamics of the diffusing pathogens to that of human population in the jth patch, we substitute (15) into the ODE system (7c) to obtain

$$\frac{dS_j}{dt} = -\sum_{i=1}^{m} \beta_i S_j \gamma_{ji} \left(p(t) + \frac{\sigma_i I_i}{2\pi D_0}\right) - \frac{\nu}{D_0} \sum_{i=1}^{m} \beta_i S_j \gamma_{ji} \, \Psi_i$$

$$\frac{dI_j}{dt} = \sum_{i=1}^{m} \beta_i S_j \gamma_{ji} \left(p(t) + \frac{\sigma_i I_i}{2\pi D_0}\right) - \frac{\nu}{D_0} \sum_{i=1}^{m} \beta_i S_j \gamma_{ji} \, \Psi_i - \phi_j I_j \qquad (16)$$

$$\frac{dR_j}{dt} = \phi_j I_j, \qquad j = 1, \ldots, m,$$

where $\Psi_j = (\mathcal{G}\Phi)_j$ is the jth entry of the vector $\mathcal{G}\Phi$, with $\Phi = (\sigma_1 I_1, \ldots, \sigma_m I_m)^T$. Here, $\mathcal{G}$ is the Neumann–Green's matrix whose entries are defined by

$$(\mathcal{G})_{jj} = \Re(\boldsymbol{x}_j) \quad \text{for} \quad i = j \quad \text{and} \quad (\mathcal{G})_{ij} = (\mathcal{G})_{ji} = G(\boldsymbol{x}_i; \boldsymbol{x}_j) \quad \text{for} \quad i \neq j, \quad (17)$$

where $G(\boldsymbol{x}_j; \boldsymbol{x}_i)$ is the Neumann–Green's function satisfying (13) and $\Re_j \equiv \Re(\boldsymbol{x}_j)$ is its regular part at the point $\boldsymbol{x} = \boldsymbol{x}_j$. For convenience of notation, we have replaced $P_0(t)$ with $p(t)$ in (16). Combining (12) and (16), we obtain an ODE systems for the average density of pathogen in the atmosphere coupled to the population dynamics in the patches that is valid in the limit $D = O(\nu^{-1})$, where $\nu = -1/\log(\varepsilon)$ with $\varepsilon \ll 1$. This ODE system is given by

$$\frac{dp(t)}{dt} = -p(t) + \frac{1}{|\Omega|} \sum_{j=1}^{m} \sigma_j I_j, \qquad\qquad\qquad\qquad (18a)$$

$$\frac{dS_j}{dt} = -\sum_{i=1}^{m} \beta_i S_j \gamma_{ji} \left(p(t) + \frac{\sigma_i I_i}{2\pi D_0}\right) - \frac{\nu}{D_0} \sum_{i=1}^{m} \beta_i S_j \gamma_{ji} \, \Psi_i, \qquad (18b)$$

$$\frac{dI_j}{dt} = \sum_{i=1}^{m} \beta_i S_j \gamma_{ji} \left(p(t) + \frac{\sigma_i I_i}{2\pi D_0}\right) - \frac{\nu}{D_0} \sum_{i=1}^{m} \beta_i S_j \gamma_{ji} \, \Psi_i - \phi_j I_j, \qquad (18c)$$

$$\frac{dR_j}{dt} = \phi_j I_j, \qquad\qquad j = 1, \ldots, m. \qquad\qquad\qquad (18d)$$

Note that the terms with $\sigma_j I_j/(2\pi D_0)$ in (18) do not model direct transmission, but rather they account for the pathogens shed by infected individuals in the jth patch. The density of these pathogens depends on the scaled-diffusion rate D_0 and the population of infected individuals in the patch. When the pathogens diffuse slowly (small D_0), there is significant contribution from this term, and this contribution decreases as D_0 increases. In the limit $D_0 \to \infty$, these terms go to zero and the ODE system reduces to the model for well-mixed regime present in equation 5 of Funke (2018). In Sects. 3,

we study the reduced ODE system (18) for two population patches and compute the basic reproduction number and final size relation for this scenario.

3 Two-Patch Model with Heterogeneous Mixing

In this section, we consider a scenario with two population patches ($m = 2$) centered at $x_1 = (0.5, 0)$ and $x_2 = (-0.5, 0)$ in the unit disk and use the dimensionless coupled PDE–ODE model (7) and the reduced system of ODEs (18) to study the dynamics of the disease in these populations. For this scenario, we derive from (7) that the dimensionless density of pathogens $P(x, t)$ in the atmosphere satisfies

$$\frac{\partial P}{\partial t} = D \Delta P - P, \quad t > 0, \quad x \in \Omega \setminus \{\Omega_1 \cup \Omega_2\}; \tag{19a}$$

$$\partial_n P = 0, \quad x \in \partial\Omega; \quad 2\pi\varepsilon D \, \partial_n P = -\sigma_1 I_1, \quad x \in \partial\Omega_1;$$

$$2\pi\varepsilon D \, \partial_n P = -\sigma_2 I_2, \quad x \in \partial\Omega_2, \tag{19b}$$

where Ω_1 and Ω_2 are the two population patches centered at $x_1 = (0.5, 0)$ and $x_2 = (-0.5, 0)$, respectively. The dynamics of the diffusion pathogens is coupled to the population dynamics of the two patches as follows

Patch 1   **Patch 2**

$$\frac{dS_1}{dt} = -\frac{1}{2\pi\varepsilon} \sum_{i=1}^{2} \beta_i \, S_1 \, \gamma_{1i} \int_{\partial\Omega_{\varepsilon_i}} P \, ds_x; \qquad \frac{dS_2}{dt} = -\frac{1}{2\pi\varepsilon} \sum_{i=1}^{2} \beta_i \, S_2 \, \gamma_{2i} \int_{\partial\Omega_{\varepsilon_i}} P \, ds_x;$$

$$\frac{dI_1}{dt} = \frac{1}{2\pi\varepsilon} \sum_{i=1}^{2} \beta_i \, S_1 \, \gamma_{1i} \int_{\partial\Omega_{\varepsilon_i}} P \, ds_x - \phi_1 I_1; \qquad \frac{dI_2}{dt} = \frac{1}{2\pi\varepsilon} \sum_{i=1}^{2} \beta_i \, S_2 \, \gamma_{2i} \int_{\partial\Omega_{\varepsilon_i}} P \, ds_x - \phi_2 I_2;$$

$$\frac{dR_1}{dt} = \phi_1 I_1; \qquad\qquad\qquad\qquad\qquad \frac{dR_2}{dt} = \phi_2 I_2. \tag{19c}$$

Similarly, we derive the reduced ODE system for the two population patch scenario from (18) as

$$\frac{dp}{dt} = -p + \frac{1}{|\Omega|} (\sigma_1 I_1 + \sigma_2 I_2), \tag{20a}$$

Patch 1   **Patch 2**

$$\frac{dS_1}{dt} = -\sum_{i=1}^{2} \beta_i \, S_1 \, \gamma_{1i} \left(p(t) + \frac{\sigma_i I_i}{2\pi D_0} \right), \qquad \frac{dS_2}{dt} = -\sum_{i=1}^{2} \beta_i \, S_2 \, \gamma_{2i} \left(p(t) + \frac{\sigma_i I_i}{2\pi D_0} \right),$$

$$\frac{dI_1}{dt} = \sum_{i=1}^{2} \beta_i \, S_1 \, \gamma_{1i} \left(p(t) + \frac{\sigma_i I_i}{2\pi D_0} \right) - \phi_1 I_1, \qquad \frac{dI_2}{dt} = \sum_{i=1}^{2} \beta_i \, S_2 \, \gamma_{2i} \left(p(t) + \frac{\sigma_i I_i}{2\pi D_0} \right) - \phi_2 I_2,$$

$$\frac{dR_1}{dt} = \phi_1 I_1, \qquad\qquad\qquad\qquad\qquad \frac{dR_2}{dt} = \phi_2 I_2, \tag{20b}$$

where $p \equiv p(t)$ is the average density of pathogens in the atmosphere and D_0 is the scaled diffusion coefficient of the pathogens. The ODE system (20) has a similar struc-

ture to those studied in David et al. (2020) and Funke (2018). The coupled PDE–ODE model (19), and the reduced ODE system (20) will be used to study the transmission dynamics of the disease for two populations scenario.

3.1 Basic Reproduction Number

Here, we use the reduced system of ODEs (20) to compute the basic reproduction number, $\mathcal{R}_0$ (the secondary infections caused by a single infective into a totally susceptible population). To use the next generational matrix approach for computing $\mathcal{R}_0$ as was done in Odo et al. (1990), Holland (2007) and Van den Driessche and Watmough (2002), we construct a system of equations for the infectious classes given by

$$
\begin{aligned}
\frac{dI_1}{dt} &= \beta_1 S_1 \gamma_{11} \left(p(t) + \frac{\sigma_1 I_1}{2\pi D_0} \right) + \beta_2 S_1 \gamma_{12} \left(p(t) + \frac{\sigma_2 I_2}{2\pi D_0} \right) - \phi_1 I_1, \\
\frac{dI_2}{dt} &= \beta_1 S_2 \gamma_{21} \left(p(t) + \frac{\sigma_1 I_1}{2\pi D_0} \right) + \beta_2 S_2 \gamma_{22} \left(p(t) + \frac{\sigma_2 I_2}{2\pi D_0} \right) - \phi_2 I_2, \quad (21) \\
\frac{dp}{dt} &= -p + \frac{1}{|\Omega|} (\sigma_1 I_1 + \sigma_2 I_2),
\end{aligned}
$$

where γ_{11} and γ_{12} are the proportions of the residence of patch 1 that are currently in patch 1 and patch 2, respectively, with $\gamma_{11} + \gamma_{12} = 1$. Similarly, γ_{21} and γ_{22} are the proportions of the residence of patch 2 that are currently in patch 1 and patch 2, respectively, with $\gamma_{21} + \gamma_{22} = 1$.

At the disease-free equilibrium DFE $= (S_1^*, I_1^*, R_1^*, S_2^*, I_2^*, R_2^*, p^*) \equiv (S_1(0), 0, 0, S_2(0), 0, 0, 0)$, we construct the Jacobian matrix F for new infections and the matrix V for transfer of infections. Since $I_1(0) = I_2(0) = R_1(0) = R_2(0) = 0$, at the DFE, we have $S_1^* = N_1(0)$ and $S_2^* = N_2(0)$. Based on this, the matrix F is given by

$$
F = \left(\frac{\partial \mathcal{F}_i}{\partial x_j} \right)_{i,j} = \begin{pmatrix} \dfrac{\sigma_1 \beta_1 \gamma_{11} N_1(0)}{2\pi D_0} & \dfrac{\sigma_2 \beta_2 \gamma_{12} N_1(0)}{2\pi D_0} & (\beta_1 \gamma_{11} + \beta_2 \gamma_{12}) N_1(0) \\[3mm] \dfrac{\sigma_1 \beta_1 \gamma_{21} N_2(0)}{2\pi D_0} & \dfrac{\sigma_2 \beta_2 \gamma_{22} N_2(0)}{2\pi D_0} & (\beta_1 \gamma_{21} + \beta_2 \gamma_{22}) N_2(0) \\[3mm] 0 & 0 & 0 \end{pmatrix}, \quad (22)
$$

where the functions $(\mathcal{F}_1, \mathcal{F}_2, \mathcal{F}_2) \equiv (I_1', I_2', p')$ are as given in (21) with $(x_1, x_2, x_3) \equiv (I_1, I_2, p)$. Similarly, from (21), we construct the Jacobian matrix V for the rates of transfer of individuals between the infected compartments as

$$V = \left(\frac{\partial \mathcal{V}_i}{\partial x_j}\right)_{i,j} = \begin{pmatrix} \phi_1 & 0 & 0 \\ 0 & \phi_2 & 0 \\ -\dfrac{\sigma_1}{|\Omega|} & -\dfrac{\sigma_2}{|\Omega|} & 1 \end{pmatrix}. \tag{23}$$

Upon finding the inverse of V and multiplying by F (22) from the left, we obtain the next generation matrix defined by $\mathcal{M} = FV^{-1}$. Our desired basic reproduction number is the spectral radius of the next generation matrix. Computing the eigenvalues of this matrix, we obtain the basic reproduction number of our model as

$$\mathcal{R}_0 = \frac{\mho_{11} + \mho_{22}}{4\pi\phi_1\phi_2|\Omega|D_0} + \frac{\sqrt{\mho_{11}^2 + \Upsilon + \mho_{22}^2}}{2\phi_1\phi_2}, \tag{24}$$

where $\mho_{11}$, $\mho_{22}$, and Υ are defined as follows

$$\mho_{11} = (2\pi D_0(\beta_1\gamma_{11} + \beta_2\gamma_{12}) + \beta_1\gamma_{11}|\Omega|) N_1(0)\phi_2\sigma_1,$$
$$\mho_{22} = (2\pi D_0(\beta_1\gamma_{21} + \beta_2\gamma_{22}) + \beta_2\gamma_{22}|\Omega|) N_2(0)\phi_1\sigma_2,$$
$$\Upsilon = 2\phi_1\phi_2\sigma_1\sigma_2 N_1(0) N_2(0) \left(\frac{(\beta_1\gamma_{11} + \beta_2\gamma_{12})}{2\pi D_0|\Omega|^2}\mho_{22}^- - \frac{\beta_1\gamma_{11}}{4\pi^2 D_0^2|\Omega|}\mho_{22}\right.$$
$$\left. + \frac{\beta_1\gamma_{21}}{4\pi^2 D_0^2|\Omega|}\mho_{12}^- + \frac{\beta_2\gamma_{12}}{4\pi^2 D_0^2|\Omega|}\mho_{21}^-\right). \tag{25}$$

Here, the variables $\mho_{22}^-$, $\mho_{12}^-$ and $\mho_{21}^-$ are given by

$$\mho_{22}^- = \left(2\pi D_0(\beta_1\gamma_{21} + \beta_2\gamma_{22}) - \beta_2\gamma_{22}|\Omega|\right),$$
$$\mho_{12}^- = \left(4\pi D_0(\beta_1\gamma_{11} + \beta_2\gamma_{12}) + \beta_2\gamma_{12}|\Omega|\right), \tag{26}$$
$$\mho_{21}^- = \left(4\pi D_0(\beta_1\gamma_{21} + \beta_2\gamma_{22}) + \beta_1\gamma_{21}|\Omega|\right),$$

To better understand the basic reproduction number $\mathcal{R}_0$ (24), we consider some limiting scenarios and make simplifying assumptions on the mixing pattern between the two populations:

1. In the well-mixed limit, where $D_0 \to \infty$, the basic reproduction number in (24) reduces to

$$\mathcal{R}_0^\infty = (\beta_1\gamma_{11} + \beta_2\gamma_{12})\mathcal{R}_1 + (\beta_1\gamma_{21} + \beta_2\gamma_{22})\mathcal{R}_2, \tag{27}$$

where $\mathcal{R}_1 = N_1(0)\sigma_1/(\phi_1|\Omega|)$ and $\mathcal{R}_2 = N_2(0)\sigma_2/(\phi_2|\Omega|)$. The first term in (27) given by $(\beta_1\gamma_{11} + \beta_2\gamma_{12})\mathcal{R}_1$ accounts for the secondary infections caused indirectly by a quantity σ_1 of the pathogen shed by a single infected individual in

patch 1 per unit time for a time period $1/\phi_1$. A similar explanation holds for the second term in (27) given by $(\beta_1 \gamma_{21} + \beta_2 \gamma_{22}) \mathcal{R}_2$, but in terms of patch 2.

2. For a symmetric proportionate mixing pattern, where $\gamma_{11} = \gamma_{21} = \gamma_1$, and $\gamma_{12} = \gamma_{22} = \gamma_2$, with $\gamma_1 + \gamma_2 = 1$ and $\gamma_{11} \gamma_{22} - \gamma_{12} \gamma_{21} = 0$, the reproduction number in (27) becomes

$$\mathcal{R}_0^\infty = \frac{(\beta_1 \gamma_1 + \beta_2 \gamma_2)N_1(0)\sigma_1}{\phi_1 |\Omega|} + \frac{(\beta_1 \gamma_1 + \beta_2 \gamma_2)N_2(0)\sigma_2}{\phi_2 |\Omega|}. \tag{28}$$

3. When there is no mobility, that is, the members of each patch only mix with individuals in their patch, we have $\gamma_{11} = \gamma_{22} = 1$ (consequently, $\gamma_{12} = \gamma_{21} = 0$). Therefore, the reproduction number in (27) reduces to

$$\mathcal{R}_0^\infty = \frac{\beta_1 N_1(0)\sigma_1}{\phi_1 |\Omega|} + \frac{\beta_2 N_2(0)\sigma_2}{\phi_2 |\Omega|}. \tag{29}$$

Note that this scenario is the same as that of section 4 of David et al. (2020), and the reduced reproduction number (29) for this scenario is the same as equation 4.9 of David et al. (2020).

Our numerical simulations will give further explanations of $\mathcal{R}_0$ (for the case where $D_0 = O(1)$) and $\mathcal{R}_0^\infty$ (for the well-mixed limit $D_0 \to \infty$). We summarize the implications of the reproduction number $\mathcal{R}_0^\infty$ in the following easily proved theorem.

Theorem 1 *For system (20), the infection dies out whenever $\mathcal{R}_0^\infty < 1$, while the disease remains stable in the community but not cause an epidemic whenever $\mathcal{R}_0^\infty = 1$. Contrarily, an epidemic occurs whenever $\mathcal{R}_0^\infty > 1$.*

3.2 Final Size Relation

To represent the epidemic size in terms of the basic reproduction number and the model parameters, we derive a final size relation for the two-patch epidemic model (18). Following the approach used in Arino and Brauer (2007), Brauer (2008a), Brauer (2008b), Brauer (2017a), Brauer (2017b), Brauer (2019), Brauer and Castillo-Chaavez (2012), Brauer et al. (2018), David et al. (2020) and Funke (2018), we obtain

$$\begin{aligned} \log \frac{S_{1,0}}{S_{1,\infty}} = {} & (\beta_1 \gamma_{11} + \beta_2 \gamma_{12}) \, p_0 + (\beta_1 \gamma_{11} + \beta_2 \gamma_{12}) \mathcal{R}_1 \left\{ 1 - \frac{S_{1,\infty}}{N_1(0)} \right\} \\ & + \frac{\sigma_1 N_1(0) \beta_1 \gamma_{11}}{2 \pi D_0 \phi_1} \left\{ 1 - \frac{S_{1,\infty}}{N_1(0)} \right\} \\ & + (\beta_1 \gamma_{11} + \beta_2 \gamma_{12}) \mathcal{R}_2 \left\{ 1 - \frac{S_{2,\infty}}{N_2(0)} \right\} + \frac{\sigma_2 N_2(0) \beta_2 \gamma_{12}}{2 \pi D_0 \phi_2} \left\{ 1 - \frac{S_{2,\infty}}{N_2(0)} \right\}, \end{aligned} \tag{30a}$$

and

$$
\begin{aligned}
\log \frac{S_{2,0}}{S_{2,\infty}} =&(\beta_1 \gamma_{21} + \beta_2 \gamma_{22}) p_0 + (\beta_1 \gamma_{21} + \beta_2 \gamma_{22}) \mathcal{R}_1 \left\{ 1 - \frac{S_{1,\infty}}{N_1(0)} \right\} \\
&+ \frac{\sigma_1 N_1(0) \beta_1 \gamma_{21}}{2 \pi D_0 \phi_1} \left\{ 1 - \frac{S_{1,\infty}}{N_1(0)} \right\} \\
&+ (\beta_1 \gamma_{21} + \beta_2 \gamma_{22}) \mathcal{R}_2 \left\{ 1 - \frac{S_{2,\infty}}{N_2(0)} \right\} + \frac{\sigma_2 N_2(0) \beta_2 \gamma_{22}}{2 \pi D_0 \phi_2} \left\{ 1 - \frac{S_{2,\infty}}{N_2(0)} \right\},
\end{aligned} \tag{30b}
$$

where $\mathcal{R}_1$ and $\mathcal{R}_2$ are as defined in (27), p_0 is the initial average density of pathogens, $N_1(0)$ and $N_2(0)$ are the initial populations in patch 1 and patch 2, respectively. Here, $S_{1,0}$ and $S_{2,0}$ denote the initial susceptible populations in the patches 1 and 2, respectively, while $S_{1,\infty}$ and $S_{2,\infty}$ are the susceptible populations left in patches 1 and 2 after the outbreak. The remaining parameters are defined in Table 1.

The final size relations in (30a) and (30b) for patches 1 and 2, respectively, imply that $S_{1,\infty} > 0$ and $S_{2,\infty} > 0$. They give the relationship between the basic reproduction number R_0 and the final epidemic size in patches 1 and 2, respectively. Note that the total number of infected individuals in patches 1 and 2 over the epidemic period is, respectively, given by $N_1(0) - S_{1,\infty}$ and $N_2(0) - S_{2,\infty}$, which can be described in terms of the attack rates/ratios as $\left[1 - \dfrac{S_{1,\infty}}{N_1(0)} \right]$ and $\left[1 - \dfrac{S_{2,\infty}}{N_2(0)} \right]$ as in Brauer (2008b). The final size relation (30) takes a simpler form using the following assumptions.

1. In the case where the outbreak begins with infected individuals and no pathogens, that is, $I_1(0) \neq 0$, $I_2(0) \neq 0$ and $p_0 = 0$, the *final size relation* for patches 1 and 2 in (30a) and (30b) can be written as

$$
\begin{aligned}
\log \frac{S_{1,0}}{S_{1,\infty}} =& (\beta_1 \gamma_{11} + \beta_2 \gamma_{12}) \mathcal{R}_1 \left\{ 1 - \frac{S_{1,\infty}}{N_1(0)} \right\} + \frac{\sigma_1 N_1(0) \beta_1 \gamma_{11}}{2 \pi D_0 \phi_1} \left\{ 1 - \frac{S_{1,\infty}}{N_1(0)} \right\} \\
&+ (\beta_1 \gamma_{11} + \beta_2 \gamma_{12}) \mathcal{R}_2 \left\{ 1 - \frac{S_{1,\infty}}{N_1(0)} \right\} + \frac{\sigma_2 N_2(0) \beta_2 \gamma_{12}}{2 \pi D_0 \phi_2} \left\{ 1 - \frac{S_{2,\infty}}{N_2(0)} \right\},
\end{aligned} \tag{31}
$$

and

$$
\begin{aligned}
\log \frac{S_{2,0}}{S_{2,\infty}} =& (\beta_1 \gamma_{21} + \beta_2 \gamma_{22}) \mathcal{R}_1 \left\{ 1 - \frac{S_{1,\infty}}{N_1(0)} \right\} + \frac{\sigma_1 N_1(0) \beta_1 \gamma_{21}}{2 \pi D_0 \phi_1} \left\{ 1 - \frac{S_{1,\infty}}{N_1(0)} \right\} \\
&+ (\beta_1 \gamma_{21} + \beta_2 \gamma_{22}) \mathcal{R}_2 \left\{ 1 - \frac{S_{2,\infty}}{N_2(0)} \right\} + \frac{\sigma_2 N_2(0) \beta_2 \gamma_{22}}{2 \pi D_0 \phi_2} \left\{ 1 - \frac{S_{2,\infty}}{N_2(0)} \right\}.
\end{aligned} \tag{32}
$$

2. In the limit $D_0 \to \infty$ (well mixed), the final size relation (31) and (32) becomes

$$\log \frac{S_{1,0}}{S_{1,\infty}} = (\beta_1\,\gamma_{11} + \beta_2\,\gamma_{12})\,\mathcal{R}_1 \left\{ 1 - \frac{S_{1,\infty}}{N_1(0)} \right\} + (\beta_1\,\gamma_{11} + \beta_2\,\gamma_{12})\,\mathcal{R}_2 \left\{ 1 - \frac{S_{2,\infty}}{N_2(0)} \right\},$$
$$\log \frac{S_{2,0}}{S_{2,\infty}} = (\beta_1\,\gamma_{21} + \beta_2\,\gamma_{22})\,\mathcal{R}_1 \left\{ 1 - \frac{S_{1,\infty}}{N_1(0)} \right\} + (\beta_1\,\gamma_{21} + \beta_2\,\gamma_{22})\,\mathcal{R}_2 \left\{ 1 - \frac{S_{2,\infty}}{N_2(0)} \right\}.$$

$$(33)$$

This result can be written in a matrix form as

$$\begin{pmatrix} \log \dfrac{S_{1,0}}{S_{1,\infty}} \\[2mm] \log \dfrac{S_{2,0}}{S_{2,\infty}} \end{pmatrix} = \begin{pmatrix} \mathbb{M}_{11} & \mathbb{M}_{12} \\[1mm] \mathbb{M}_{21} & \mathbb{M}_{22} \end{pmatrix} \begin{pmatrix} 1 - \dfrac{S_{1,\infty}}{N_1(0)} \\[2mm] 1 - \dfrac{S_{2,\infty}}{N_2(0)} \end{pmatrix},$$

$$\text{where} \quad \mathbb{M} = \begin{pmatrix} (\beta_1\,\gamma_{11} + \beta_2\,\gamma_{12})\,\mathcal{R}_1 & (\beta_1\,\gamma_{11} + \beta_2\,\gamma_{12})\,\mathcal{R}_2 \\[1mm] (\beta_1\,\gamma_{21} + \beta_2\,\gamma_{22})\,\mathcal{R}_1 & (\beta_1\,\gamma_{21} + \beta_2\,\gamma_{22})\,\mathcal{R}_2 \end{pmatrix}.$$

$$(34)$$

3. If the mixing is proportionate, that is, $\gamma_{11} = \gamma_{21} = \gamma_1$, and $\gamma_{12} = \gamma_{22} = \gamma_2$, the final size relation (34) becomes

$$\begin{pmatrix} \log \dfrac{S_{1,0}}{S_{1,\infty}} \\[2mm] \log \dfrac{S_{2,0}}{S_{2,\infty}} \end{pmatrix} = \begin{pmatrix} \mathbb{N}_{11} & \mathbb{N}_{12} \\[1mm] \mathbb{N}_{21} & \mathbb{N}_{22} \end{pmatrix} \begin{pmatrix} 1 - \dfrac{S_{1,\infty}}{N_1(0)} \\[2mm] 1 - \dfrac{S_{2,\infty}}{N_2(0)} \end{pmatrix},$$

$$\text{where} \quad \mathbb{N} = \begin{pmatrix} (\beta_1\,\gamma_1 + \beta_2\,\gamma_2)\,\mathcal{R}_1 & (\beta_1\,\gamma_1 + \beta_2\,\gamma_2)\,\mathcal{R}_2 \\[1mm] (\beta_1\,\gamma_1 + \beta_2\,\gamma_2)\,\mathcal{R}_1 & (\beta_1\,\gamma_1 + \beta_2\,\gamma_2)\,\mathcal{R}_2 \end{pmatrix}.$$

$$(35)$$

4. If the mixing is like-with-like (no mobility), that is $\gamma_{11} = \gamma_{22} = 1$, and $\gamma_{12} = \gamma_{21} = 0$, the final size relation (34) reduces to

$$\begin{pmatrix} \log \dfrac{S_{1,0}}{S_{1,\infty}} \\[2mm] \log \dfrac{S_{2,0}}{S_{2,\infty}} \end{pmatrix} = \begin{pmatrix} \mathbb{W}_{11} & \mathbb{W}_{12} \\[1mm] \mathbb{W}_{21} & \mathbb{W}_{22} \end{pmatrix} \begin{pmatrix} 1 - \dfrac{S_{1,\infty}}{N_1(0)} \\[2mm] 1 - \dfrac{S_{2,\infty}}{N_2(0)} \end{pmatrix}, \quad \text{where} \quad \mathbb{W} = \begin{pmatrix} \beta_1\,\mathcal{R}_1 & \beta_1\,\mathcal{R}_2 \\[1mm] \beta_2\,\mathcal{R}_1 & \beta_2\,\mathcal{R}_2 \end{pmatrix}, \quad (36)$$

which can be written as

$$\beta_2 \, \log \frac{S_{1,0}}{S_{1,\infty}} = \beta_1 \, \log \frac{S_{2,0}}{S_{2,\infty}}. \tag{37}$$

We can further reduce (37) to obtain

$$\left[\frac{S_{1,0}}{S_{1,\infty}}\right]^{\beta_2} = \left[\frac{S_{2,0}}{S_{2,\infty}}\right]^{\beta_1} \tag{38}$$

If $\beta_1 > \beta_2$ in (38), then

$$1 - \log\frac{S_{1,0}}{S_{1,\infty}} > 1 - \log\frac{S_{2,0}}{S_{2,\infty}}, \tag{39}$$

which implies that the attack rate/ratio is greater in the more active patch.

The assumptions above and their effects on the epidemic peak and time will be explored and discussed in the numerical simulations.

3.3 Numerical Simulations

We present numerical simulations of the dimensional coupled PDE–ODE model (19) and the reduced system of ODEs (20) for two population patches. For all scenarios considered in this section, these patches are located at $\boldsymbol{x}_1 = (0.5, 0)$ and $\boldsymbol{x}_2 = (-0.5, 0)$ for patches 1 and 2, respectively, and the coupled PDE–ODE model is solved using FlexPDE6 PDE solutions Inc (2019). We aim to study the effect of pathogen diffusion and human mobility on the disease dynamics in an heterogeneous mixing environment.

In Fig. 1, we used the reduced ODE system (20) to study the effect of the diffusion rate of pathogens and heterogeneous mixing between two populations on the transmission dynamics of the diseases in the populations. For the results in the left panel (initial conditions: $S_1(0) = 299/300$, $I_1(0) = 1/300$, $R_1(0) = 0$, $S_2(0) = 249/250$, $I_2(0) = 1/250$, $R_2(0) = 0$, and $p(0) = 0$), we have only infected individuals with no pathogens at the beginning of the outbreak, while for those in the right panel (initial conditions: $S_1(0) = 300/300$, $I_1(0) = 0$, $R_1(0) = 0$, $S_2(0) = 250/250$, $I_2(0) = 0$, $R_2(0) = 0$, and $p(0) = 1$), we have only diffusing pathogens with no infected individuals at the beginning of the epidemic. The second scenario, where the outbreak begins with only pathogens, can be related to a scenario where pathogens diffuse out of an infected population to a completely susceptible population. The solid and dashed curves are for patch 1 and patch 2, respectively. The black, blue, and red curves are for the scaled diffusion rates $D_0 = 0.128$, $D_0 = 2.556$, and $D_0 = 76.687$, respectively. Using the relation for D_0 and D given in (9), these scaled diffusion rates correspond to $D = 0.5$, $D = 10$, and $D = 300$, respectively.

We observe from the results in the top panel of Fig. 1 for the scenario with no human mobility ($\gamma_{11} = 1$, $\gamma_{12} = 0$, $\gamma_{21} = 0$, and $\gamma_{22} = 1$) that the epidemic peak decreases and the peak time increases, with increase in the scaled diffusion rate. Overall and in this scenario, patch 2 (dashed curves) experiences a higher peak and shorter peak time for all values of D_0 when compared to patch 1 (solid curves) due to higher transmission and shedding rates in patch 2 (see Table 1 for more details). In addition, the epidemic take-off seems delayed when the outbreak begins with some infectives and no pathogen (left panel), compared to when the outbreak begins with zero infectives and a pathogen
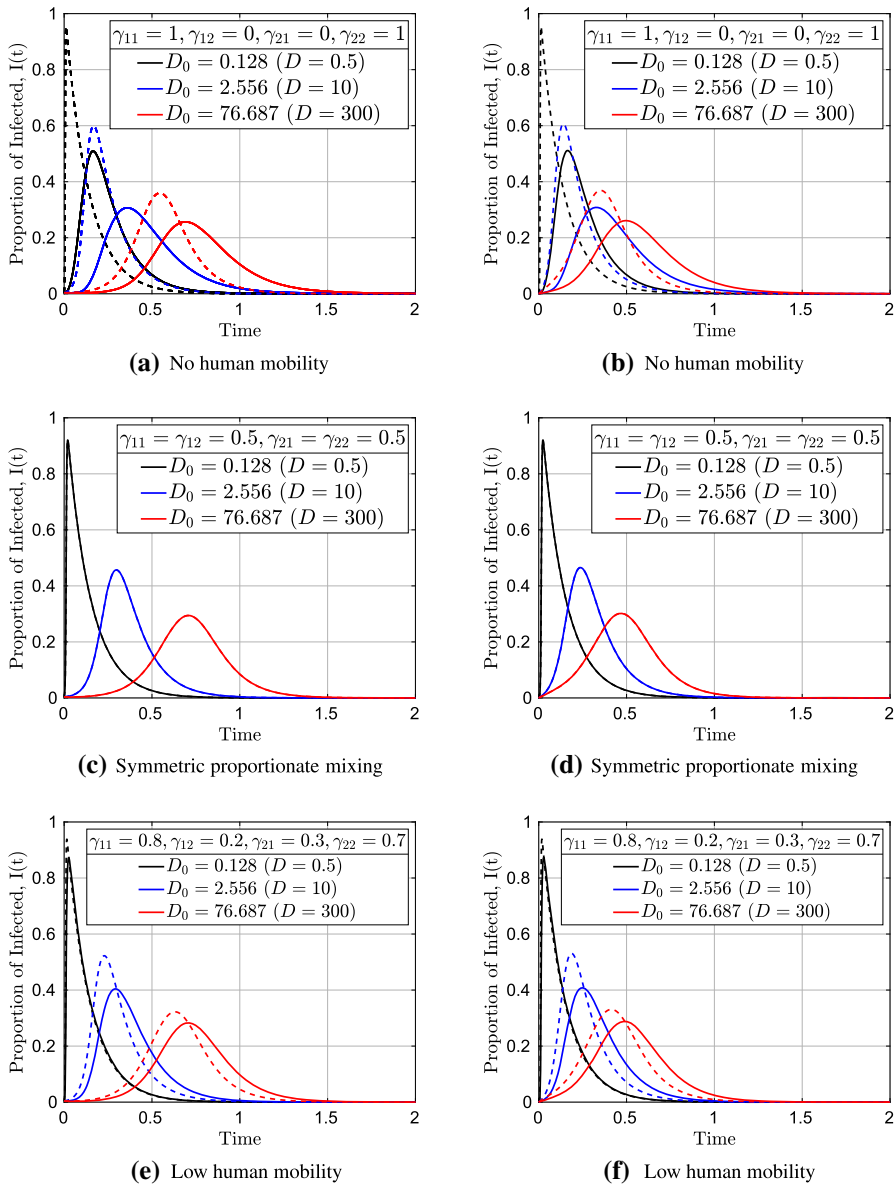
(a) No human mobility

(b) No human mobility

(c) Symmetric proportionate mixing

(d) Symmetric proportionate mixing

(e) Low human mobility

(f) Low human mobility

Fig. 1 Effect of pathogen diffusion and human mobility on disease dynamics (ODE model). Numerical simulations of the ODE system (20) for different diffusion rate of pathogens and human mobility. Left panel: infection starts with no pathogen, with initial conditions $S_1(0) = 299/300$, $I_1(0) = 1/300$, $R_1(0) = 0$, $S_2(0) = 249/250$, $I_2(0) = 1/250$, $R_2(0) = 0$, and $p(0) = 0$, and right panel: infection starts with only pathogens with initial conditions $S_1(0) = 300/300$, $I_1(0) = 0$, $R_1(0) = 0$, $S_2(0) = 250/250$, $I_2(0) = 0$, $R_2(0) = 0$, and $p(0) = 1$. Top row: no human mobility ($\gamma_{11} = 1$, $\gamma_{12} = 0$, $\gamma_{21} = 0$, and $\gamma_{22} = 1$), middle row: symmetric proportionate mixing ($\gamma_{11} = \gamma_{12} = 0.5$ and $\gamma_{21} = \gamma_{22} = 0.5$), and bottom row: non-symmetric proportionate mixing (low mobility: $\gamma_{11} = 0.8$, $\gamma_{12} = 0.2$ and $\gamma_{21} = 0.3$, $\gamma_{22} = 0.7$). All other parameters are given in Table 1. Solid curves are for patch 1 while the dashed curves are for patch 2. Note that the solid and dashed curves are overlapping for the results in the middle row (Color figure online)

Table 1 Model parameters, descriptions, and values

Parameter	Description	Patch 1, 2 values	References
μ	Dimensional effective contact rate	0.3, 1.2	Bichara et al. (2015)
β	Dimensionless effective contact rate	Computed using (8)	Derived
r	Dimensional pathogen shedding rate	0.1, 1	Zhang et al. (2016)
σ	Dimensionless pathogen shedding rate	Computed using (8)	Derived
α	Dimensional recovery rate	1.87	Zhang et al. (2016)
ϕ	Dimensionless recovery rate	Computed using (8)	Derived
N_1, N_2	Total population	300, 250	Assumed
D_B	Dimensional diffusion rate of pathogens		
D	Dimensionless diffusion rate of pathogens	Varied	
D_0	Scaled dimensionless diffusion rate of pathogens	Computed using (9)	Derived
γ_{11}	Fraction of patch 1 residents currently in patch 1	Varied	
γ_{12}	Fraction of patch 1 residents currently in patch 2	Varied	
γ_{21}	Fraction of patch 2 residents currently in patch 1	Varied	
γ_{22}	Fraction of patch 2 residents currently in patch 2	Varied	
δ	Dimensionless decay rate of pathogens	0.25	Assumed
p_c	Typical value for density of pathogens	0.01	Assumed
ε	Radius of the population patch	0.02	Assumed
$|\Omega|$	Area of the domain (unit disk)	π	Derived

(right panel). This observation is more apparent when the diffusion rate is increases (blue and red curves).

Similar results obtained using the full coupled PDE–ODE model (19) are given in the top panel of Fig. 2. In the middle panel of Fig. 1, we have the results for the case of symmetric proportional mixing ($\gamma_{11} = \gamma_{12} = 0.5$ and $\gamma_{21} = \gamma_{22} = 0.5$). For this scenario, the activity level in the two populations is assumed to be the same, and as a result, an equal proportion of the two population are mixing at all time. As observed from the results in the middle panel of Fig. 1, this mixing patterns lead to a well-mixed (homogeneous) system. Even though the transmission and shedding rates of patch 2 are higher than those of patch 1, our numerical simulations predict identical epidemics for the two populations.

In the bottom panel of Fig. 1, we consider the case of non-symmetric proportionate mixing (low mobility). For this example, we assume that 80% of the residents of patch 1 mix with only the individuals in their patch, while the remaining 20% mix with residents of patch 2 ($\gamma_{11} = 0.8$, $\gamma_{12} = 0.2$). On the other hand, we assume 70% of the residents of patch 2 mix with only members of their patch, while the remaining 30% mix with residents of patch 1 ($\gamma_{21} = 0.3$, $\gamma_{22} = 0.7$). We observe from the results for this scenario (bottom panel of Fig. 1) that the epidemic peak is higher in patch 2 (dashed curves) compared to patch 1 (solid curves) due to higher transmission and shedding rates in patch 2. In this scenario, we say that the residence of patch 2 is having more activities than those in patch 1 since a larger fraction of them is mixing with the individuals in patch 1 than those of patch 1 are mixing with them.

Comparing the results in the top (no mobility) and bottom (low mobility) panels of Fig. 1, we notice that there is an increase in the epidemic peaks for patch 1 when there is mobility compared to when there is no mobility (top panel). These differences in the epidemic size between the two scenarios are due to the heterogeneous mixing between the two populations. On the other hand, there is a slight decrease in the epidemic peaks for patch 2 when there is mobility (bottom panel) compared to when there is no mobility (top panel). For all the scenarios considered in Fig. 1, similar results computed using the full PDE model (19) are presented in Fig. 2. Both results agree well.

The results in Fig. 3 are used to study the effect of heterogeneous mixing on the disease dynamics for a fixed diffusion rate of pathogens, $D = 10$ (corresponding to $D_0 = 2.556$). The initial conditions used are $S_1(0) = 299/300$, $I_1(0) = 1/300$, $R_1(0) = 0$, $S_2(0) = 249/250$, $I_2(0) = 1/250$, $R_2(0) = 0$, and $p(0) = 1$, with other parameters as given in Table 1. Similar to the results presented in Figs. 1 and 2, the solid and dashed curves are for patch 1 and patch 2, respectively. The results in the left panel were obtained using the reduced ODE system (20) and those in right panel were obtained using the coupled PDE–ODE model (19). The black curves show the results for when there is no movement between the two populations, the blue curves are for symmetric proportionate mixing, where half of the two populations are mixing, while the red curves are for non-symmetric proportionate mixing (low mobility). We observe from these results that the no mixing scenario predicts the most difference in the epidemics of the two populations. When there is a symmetric proportionate mixing, an identical epidemic is predicted for the two populations, irrespective of the difference in their transmission and shedding rates. Lastly, for the case of non-
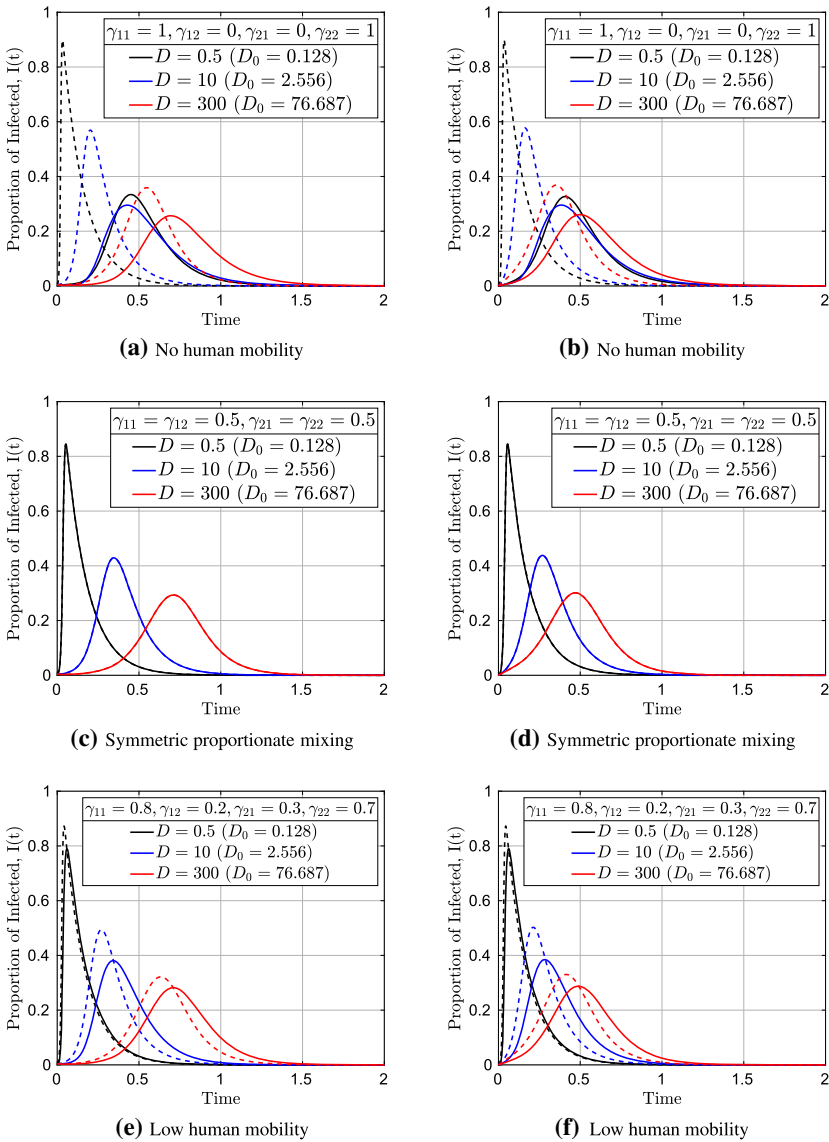
Fig. 2 Effect of pathogen diffusion and human mobility on disease dynamics (PDE–ODE model). Numerical simulations of the full PDE–ODE model (19) for different diffusion rate of pathogens and human mobility. Left panel: infection starts with no pathogen, with initial conditions $S_1(0) = 299/300$, $I_1(0) = 1/300$, $R_1(0) = 0$, $S_2(0) = 249/250$, $I_2(0) = 1/250$, $R_2(0) = 0$, and $p(0) = 0$, and right panel: infection starts with only pathogens with initial conditions $S_1(0) = 300/300$, $I_1(0) = 0$, $R_1(0) = 0$, $S_2(0) = 250/250$, $I_2(0) = 0$, $R_2(0) = 0$, and $p(0) = 1$. Top row: no human mobility ($\gamma_{11} = 1$, $\gamma_{12} = 0$, $\gamma_{21} = 0$, and $\gamma_{22} = 1$), middle row: symmetric proportionate mixing ($\gamma_{11} = \gamma_{12} = 0.5$ and $\gamma_{21} = \gamma_{22} = 0.5$), and bottom row: non-symmetric proportionate mixing (low mobility: $\gamma_{11} = 0.8$, $\gamma_{12} = 0.2$ and $\gamma_{21} = 0.3$, $\gamma_{22} = 0.7$). All other parameters are given in Table 1. Solid curves are for patch 1 while the dashed curves are for patch 2. Note that the solid and dashed curves are overlapping for the results in the middle row (Color figure online)
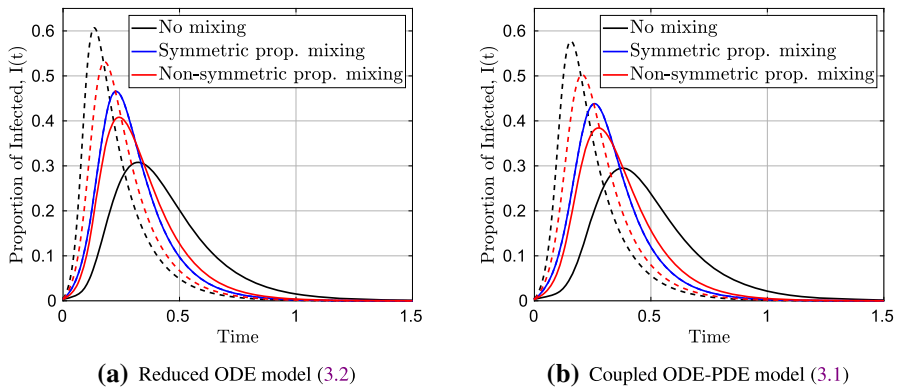
(a) Reduced ODE model (3.2)   **(b)** Coupled ODE-PDE model (3.1)

Fig. 3 Effect of population mixing patterns on disease dynamics. Numerical simulations of the ODE system (20) (left panel) and the coupled PDE–ODE model (19) (right panel) for two population patches and different population mixing patterns. The solid and dashed curves are for patch 1 and patch 2, respectively. The black, blue, and red curves are, respectively, for the scenarios with no mobility ($\gamma_{11} = 1$, $\gamma_{12} = 0$, $\gamma_{21} = 0$, and $\gamma_{22} = 1$), symmetric mixing ($\gamma_{11} = \gamma_{12} = 0.5$ and $\gamma_{21} = \gamma_{22} = 0.5$) and non-symmetric proportionate mixing (low mobility: $\gamma_{11} = 0.8$, $\gamma_{12} = 0.2$ and $\gamma_{21} = 0.3$, $\gamma_{22} = 0.7$). The initial conditions used are $S_1(0) = 299/300$, $I_1(0) = 1/300$, $R_1(0) = 0$, $S_2(0) = 249/250$, $I_2(0) = 1/250$, $R_2(0) = 0$, and $p(0) = 1$. For the PDE–ODE model, we used $D = 10$ (right panel), corresponding to $D_0 = 2.556$ for the reduce ODE system (left panel). All other parameters are given in Table 1 (Color figure online)

symmetric mixing, there is a decrease in the epidemic for the population with higher shedding and transmission rates (patch 1) and an increase in the epidemic for the other population with lower transmission and shedding rates (patch 2). Comparing the results in the left and right panel of Fig. 3, we notice that the results from the reduced system of ODEs (20) agree well with those obtained using the full coupled PDE–ODE model (19). This shows that the reduced ODE system provides a good approximation for the coupled PDE–ODE system.

4 Discussion

We have extended the novel coupled PDE–ODE model developed in David et al. (2020) for studying the transmission dynamics of airborne diseases to include human mobility. Human mobility between populations was incorporated using the Lagrangian approach. This model is used to study the indirect transmission of airborne diseases, where a susceptible individual becomes infected after coming in contact with pathogens. Infected individuals shed pathogens into the environment at some rate, and the pathogens diffuse and decay in the environment at constant rates. In the limit of fast diffusing pathogens, matched asymptotic analysis was used to reduce the PDE–ODE model to a nonlinear system of ODEs for the average density of pathogens in the environment. The reduced ODEs system was then used to derive the basic reproduction number and a final size relation for the epidemic. Numerical simulations of both the coupled PDE–ODE model and the reduced system of ODEs were used to study the

effect of the diffusion rate of pathogens and heterogeneous mixing on the dynamics of airborne diseases.

To study the effect of heterogeneous mixing between populations, we considered two non-identical population patches centered at $(0.5, 0)$ and $(-0.5, 0)$ for patches 1 and 2, respectively. The differences between the two patches were introduced through the transmission and shedding rates, where patch 2 has higher transmission and shedding rates relative to patch 1. In addition, we considered three mobility scenarios: no mobility, symmetric proportionate mixing (half populations moving), and non-symmetric proportionate mixing (low mobility). The results of our simulations show that even though the two populations are non-identical, symmetric mixing pattern leads to a well-mixed population with identical epidemics in the two populations, as a result of 50% of members of patch 2 (with higher transmission and shedding rates) mixing with individuals in patch 1 and vice versa. For non-symmetric proportionate mixing, we assumed that 80% of the individuals in patch 1 have contact with only those in patch 1, while the remaining 20% of the population have contacts with those in patch 2. On the other hand, 70% of the population of patch 2 have contact with only those in patch 2, while the remaining 30% have contact with only those in patch 1. For this mobility pattern, our numerical simulations show an increase in the epidemic in patch 1 (the patch with smaller shedding and transmission rates) compared to when there is no movement. We believe that this increase in the epidemic is due to the contacts made with individuals in patch 2 by 20% of those in patch 1, since patch 2 has higher transmission and shedding rates. These contacts would not have occurred if there was no movement. Similarly, the epidemic in patch 2 is noticed to decrease for non-symmetric mixing compared to when there is no movement, as a result of 30% of individuals in patch 2 mixing with only those in patch 1. Overall, our results show that movement between human populations may lead to an increase or decrease in the epidemic size depending on the outbreak situation and infection rate in the home or destination patch. In addition, they show that movement may be allowed from the population with high transmission and shedding rate to the other populations with lower rates, but not vice versa.

To study the impact of the diffusing pathogens on the epidemic, we consider two scenarios: when an outbreak starts with infected individuals only and when the outbreak starts with only diffusing pathogens. The latter scenario can be seen as a scenario where pathogens diffuse to completely susceptible populations from infectious populations. Our numerical simulations show that the epidemic takes off faster when the outbreak begins with diffusing pathogens compared to when it begins with infected individuals. Epidemic take-off seems delayed when the outbreak begins with infected individuals because of the time needed to shed enough pathogens that will further infect others. We also explore how the diffusion rate of pathogens impacts the disease dynamics. We solved the reduced system of ODEs and the coupled PDE–ODE model with small, moderate, and high diffusion rates of pathogens. Our results show that an increase in the diffusion rate of pathogens leads to a lower epidemic peak, and an increase in the epidemic time. Having a high diffusion rate, which may be interpreted as having a windy situation that blows the pathogens around in the air randomly, may lead to the pathogens being blown away from the settlements by the wind, there by leading to a decrease in cases. Although the analysis used to obtain our reduced system

of ODEs is only valid in the limit of fast diffusing pathogens, we observe from our numerical simulations that the results obtained using the ODE model agree well with those of the full coupled PDE–ODE model, even for small diffusion rates of pathogens. This suggests that the reduced ODE system can be used to study the disease dynamics instead of the more complicated PDE–ODE model. An important and unique feature of the ODE system is that it includes a diffusion parameter, which can be used to study the effect of diffusion of pathogen on the disease dynamics.

Summarily, the numerical simulations for both the coupled model and the reduced system of ODEs predict a change in the epidemic peak size and time with human mobility and diffusion. Our results show a decrease in the epidemic peak and an increase in the epidemic time as the diffusion rate of pathogens increases in both the coupled PDE–ODE model and the reduced system of ODEs. In the absence of movement, the epidemic is higher in the patch with higher transmission and shedding rates. In addition, when infections start with no pathogens in the air, the model predicts a delay in the epidemic take-off time relative to when infections start with pathogens, and this delay increases as the diffusion rate of pathogens increases. Our primary results show that accounting for human mobility in a heterogeneous environment is a great way to account for diseases spread in this heterogeneous world, and it is indeed worth considering. We have a similar result with David et al. (2020) when there is no human mobility between patches, and Bichara et al. (2015), where they considered only direct transmission pathway.

There are several future directions to the modeling framework presented in this paper. In this study, we assume that infections can only take place when individuals are in the patches and not outside the population patches (in the bulk region). An interesting extension of this work is to allow for infections to take place in the bulk region, which will change the model to a reaction-diffusion system. It would also be worthwhile to extend the model to include direct transmission of infections from host–host. We have considered only the leading-order terms for the reduced ODE system in this study. It would be interesting to include the $O(\nu)$ terms that incorporate the effect of the location of patches into the ODE systems. In this instance, the basic reproduction number and final size relation derived from the ODE system will depend on the location of the patches. It is straightforward to extend our current model to an n-patch model to study the impact of human mobility on disease prevalence among multiple regions. Another interesting future direction is to include interventions such as vaccination and treatment, especially in an extreme mobility scenario. Furthermore, considering the unpredictable and stochastic effect from the wind over time, a limitation of our study includes the inability to explicitly model the diffusion of pathogens in the population patches. We know that in real-world scenarios, pathogens would need to diffuse into the population before infections can take place and this diffusion process may be non-constant. We accounted for this limitation by giving scenarios of changes in the diffusion rate of pathogens and measure their effect on the disease dynamics. A possible future work in this direction will be to adapt a time-dependent diffusion term using some stochastic processes. Despite these limitations, our modeling framework provides insights into the potential impact of human mobility on the dynamics of airborne diseases. Our results give insights on boarder control (closing and opening of boarders) between two regions during a pandemic, such as COVID-19 (Yuan et al.

2022). Our study serves as a foundation for other studies and its framework can be applied to modeling other infectious diseases.

Declarations

Conflict of interest The authors declare that there is no conflict of interest.

References

Arino J, Brauer F, Van Den Driessche P, James W, Wu J (2007) A final size relation for epidemic models. Math Biosci Eng 4(2):159

Bichara D, Kang Y, Castillo-Chavez C, Horan R, Perrings C (2015) Sis and sir epidemic models under virtual dispersal. Bull Math Biol 77(11):2004–2034

Boone SA, Gerba CP (2007) Significance of fomites in the spread of respiratory and enteric viral disease. Appl Environ Microbiol 73(6):1687–1696

Brauer F (2008) Age-of-infection and the final size relation. Math Biosci Eng 5(4):681–690

Brauer F (2008) Epidemic models with heterogeneous mixing and treatment. Bull Math Biol 70(7):1869

Brauer F (2012) Heterogeneous mixing in epidemic models. Can Appl Math Q 20(1):1–13

Brauer F (2017) A final size relation for epidemic models of vector-transmitted diseases. Infect Disease Model 2(1):12–20

Brauer F (2017) A new epidemic model with indirect transmission. J Biol Dyn 11(sup2):285–293

Brauer F (2019) The final size of a serious epidemic. Bull Math Biol 81(3):869–877

Brauer F, Castillo-Chaavez C (2012) Mathematical models for communicable diseases, vol 84. SIAM, Philadelphia

Brauer F, Castillo-Chavez C, Feng Z (2018) Mathematical models in epidemiology

Carlos C-C, Derdei B, Morin BR (2016) Perspectives on the role of mobility, behavior, and time scales in the spread of diseases. Proc Natl Acad Sci 113(51):14582–14588

David JF, Iyaniwura SA, Ward MJ, Fred B (2020) A novel approach to modelling the spatial spread of airborne diseases: an epidemic model with indirect transmission. Math Biosci Eng 17(4):3294–3328

Espinoza B, Moreno V, Bichara D, Castillo-Chavez C (2016) Assessing the efficiency of movement restriction as a control strategy of ebola. In: Mathematical and statistical modeling for emerging and re-emerging infectious diseases. Springer, pp 123–145

Fred B, Carlos C-C, Zhilan F (2019) Mathematical models in epidemiology, vol 32. Springer, Berlin

Funke DJ (2018) Epidemic models with heterogeneous mixing and indirect transmission. J Biol Dyn 12(1):375–399

Hartley DM, Morris JG Jr, Smith DL (2006) Hyperinfectivity: a critical element in the ability of v. cholerae to cause epidemics? PLoS Med 3(1):e7

Holland JJ (2007) Notes on r0. Department of Anthropological Sciences, Califonia

Li Y, Huang X, Yu IT, Wong TW, Qian H (2005) Role of air distribution in sars transmission during the largest nosocomial outbreak in hong kong. Indoor Air 15(2):83–95

Lipsitch M, Cohen T, Cooper B, Robins JM, Ma S, James L, Gopalakrishna G, Chew SK, Tan CC, Samore MH et al (2003) Transmission dynamics and control of severe acute respiratory syndrome. Science 300(5627):1966–1970

Nelson EJ, Harris JB, Glenn MJ, Calderwood SB, Andrew C (2009) Cholera transmission: the host, pathogen and bacteriophage dynamic. Nat Rev Microbiol 7(10):693–702

Noakes CJ, Sleigh PA (2009) Mathematical models for assessing the role of airflow on the risk of airborne infection in hospital wards. J R Soc Interface 6(suppl–6):S791–S800

Odo D, Peter HJA, Metz JAJ (1990) On the definition and the computation of the basic reproduction ratio r 0 in models for infectious diseases in heterogeneous populations. J Math Biol 28(4):365–382

PDE solutions Inc. FlexPDE 6, 2019

Scales DC, Karen G, Chan AK, Poutanen SM, Donna F, Kylie N, Raboud JM, Refik S, Lapinsky SE, Stewart TE (2003) Illness in intensive care staff after brief exposure to severe acute respiratory syndrome. Emerg Infect Diseases 9(10):1205

Steven R, Christophe F, Donnelly CA, Ghani AC, Abu-Raddad LJ, Hedley AJ, Leung GM, Lai-Ming H, Tai-Hing L, Thach TQ et al (2003) Transmission dynamics of the etiological agent of SARS in Hong Kong: impact of public health interventions. Science 300(5627):1961–1966

Trisha G, Jimenez JL, Prather KA, Zeynep T, David F, Robert S (2021) Ten scientific reasons in support of airborne transmission of sars-cov-2. Lancet 397(10285):1603–1605

Van den Driessche P, Watmough J (2002) Reproduction numbers and sub-threshold endemic equilibria for compartmental models of disease transmission. Math Biosci 180(1–2):29–48

Wang F-B, Wang X (2021) A general multipatch cholera model in periodic environments. Discrete Continuous Dyn Syst-B

Yamazaki K, Yang C, Wang J (2021) A partially diffusive cholera model based on a general second-order differential operator. J Math Anal Appl 501(2):125181

Yuan P, Aruffo E, Li Q, Li J, Tan Y, Zheng T, David J, Ogden N, Gatov E, Gournis E et al (2022) Evaluating the risk of reopening the border: a case study of Ontario (Canada) to New York (USA) using mathematical modeling. In: Mathematics of public health. Springer, pp 287–301

Zhang L, Wang Z-C, Zhang Y (2016) Dynamics of a reaction-diffusion waterborne pathogen model with direct and indirect transmission. Comput Math Appl 72(1):202–215